

Spin reorientation by Ni doping in $\text{Cu}_{1-x}\text{Ni}_x\text{Cr}_2\text{O}_4$ spinels with $x = 0$ and 0.1 , and evidence for canted magnetic Cr order above the onset of a ferromagnetic Cu mode

N. Stüsser, M. Reehuis, M. Tovar, B. Klemke, A. Hoser, and J.-U.- Hoffmann

Helmholtz-Zentrum Berlin für Materialien und Energie, D-14109 Berlin, Germany

In ferrimagnetic spinels AB_2O_4 the magnetic structure is strongly influenced by lattice distortions, geometric frustration and the electronic properties of the cations at the A and B sites. Here, we report a comprehensive study on the temperature dependence of the magnetic structure of CuCr_2O_4 and $\text{Cu}_{0.9}\text{Ni}_{0.1}\text{Cr}_2\text{O}_4$ using neutron diffraction. CuCr_2O_4 undergoes a first continuous magnetic transition around 155 K into a canted long-range spin order on the Cr sublattice established by an antiferromagnetic and a ferromagnetic mode. Below 130 K a second transition occurs into a ferromagnetic order on the Cu sublattice resulting in a ferrimagnetic spin arrangement. Correlations between the appearance of magnetic modes and changes in the lattice geometry at different temperatures are discussed giving insight to magnetoelastic coupling. The occurrence of a ferromagnetic Cr mode above 130 K questions the common interpretation that a strong antiferromagnetic coupling between A and B spins in ferrimagnetic AB_2O_4 spinels is responsible for spin canting. From our neutron diffraction measurements of $\text{Cu}_{1-x}\text{Ni}_x\text{Cr}_2\text{O}_4$ we identify a spin reorientation for the ferromagnetic modes with a nickel content between $x = 0$ and 0.1 .

I. INTRODUCTION

Current interest in functional materials has initiated many studies on spin, lattice, and orbital degrees of freedom, especially focusing on their mutual interactions. Magnetic oxides like spinels with the general formula AB_2O_4 , belong to this class of materials. Spinel show many types of spin arrangements due to a large variety in the magnetic interactions, magnetoelastic and magnetodielectric effects, geometrical frustration etc. [1]. Normal spinels

contain $A^{2+}O_4^{2-}$ tetrahedra and $B^{3+}O_6^{2-}$ octahedra, where in the cubic structure the B ions form a pyrochlore lattice which is highly frustrated for antiferromagnetic (AF) nearest-neighbor coupling [2,3]. Lattice distortions lower the symmetry from cubic e.g. to tetragonal or orthorhombic and thereby reduce the degree of frustration. In $CuCr_2O_4$ the Jahn-Teller active Cu^{2+} ion generates a tetragonal distortion below 853 K [4,5]. A synchrotron diffraction study on $CuCr_2O_4$ reveals another lattice anomaly at about 155 K associated with a reinforcement of the tetragonal distortions. A further symmetry reduction to an orthorhombic structure sets in around 130 K, consistent with the observation of two anomalies in the temperature dependent specific heat [6]. Due to the tetragonal distortion the six identical magnetic interactions, competing between the four Cr ions on the regular tetrahedron, split into a quartet and a doublet of spin pairs with strong and weak strengths, respectively. The antiferromagnetic state is stabilized by four AF aligned spin pairs on the Cr tetrahedron and the two remaining pairs are forced into a ferromagnetic alignment (Fig. 1).

The Cu^{2+} ion at the A site has a $3d^9$ configuration with a spin-only moment of $1 \mu_B$, and the Cr^{3+} ion in the octahedral coordination has a $3d^3$ configuration with half filled t_{2g} orbitals in the high-spin state so that the spin-only moment is $3 \mu_B$. Well characterized is the ferrimagnetic (FI) ground state formed by opposing Cu and Cr moments, and the occurrence of canted magnetism on the Cr sublattice [7,8].

Recently, a magnetic phase diagram for the system $Cu_{1-x}Ni_xCr_2O_4$ has been determined by neutron diffraction indicating successive transitions [8]. For $x > 0.5$ the FI transition sets in at higher temperature followed by a transition into an AF order on the Cr sublattice. On the other hand only one magnetic transition with a simultaneous FI and AF order has been reported for $x < 0.5$ [8]. The question arises whether the two anomalies observed in the specific heat measurements originate from two subsequent magnetic transitions. This leads us to the assumption that at least the AF order sets in at higher temperature than one or both of the F modes on the Cr and Cu sublattices, respectively. This behavior differs from the sequence where a FI transition sets in first followed by AF, as is observed in many ferrimagnetic spinels with magnetic ions on the A and B position [1]. Another neutron diffraction work has been performed to investigate the two phase transitions, in particular with respect to changes in the magnetic structure [9].

Moreover, the aim of our neutron diffraction experiments is to relate possible magnetic transitions with lattice distortions in order to unravel magnetoelastic effects. Another focus is to look at the mechanism that drives the large canting of the Cr moments. The latter is frequently attributed to the competition between antiferromagnetic B - B exchange and antiferromagnetic

A - B exchange as calculated by Yafet and Kittel [10]. Mean-field calculations on possible magnetic structures of spinels, discussing also limitations of the Yafet-Kittel model, are summarized in Ref. [11]. These models also predict that systems with several transitions should enter magnetic order with a ferrimagnetic spin arrangement at the highest temperature.

II. EXPERIMENTAL, RESULTS AND DATA ANALYSIS

Experimental details on the sample preparation are given in Ref. [8]. The powder samples have grain sizes of about 20 μm sufficiently large enough for measuring pure bulk properties and small enough for ensuring random orientation of crystallites. Neutron diffraction experiments are performed on the double-focusing diffractometer E6 at the BER II reactor of the Helmholtz-Zentrum Berlin [12]. Rietveld refinements of the powder diffraction data as well as their simulations of differing magnetic structure models are carried out with the program *FullProf* [13] in a similar way as described earlier [14]. Magnetization measurements are performed on a Physical Properties Measurement System (Quantum Design operated by the Core Laboratory for Quantum Measurements at the HZB), between 5 and 200 K, applying fields corresponding to 6, 10, and 14 T.

In agreement with earlier neutron diffraction studies on CuCr_2O_4 [7,8] the magnetic structure can be described with the propagation vector $\mathbf{k} = 0$. In the ground state, a dominating AF mode on the Cr sublattice coexists with ferrimagnetism generated by two opposing ferromagnetic (F) spin modes on the individual Cu and Cr sublattices. The moment orientations for the three magnetic modes are determined by profile refinements using a diffraction pattern collected at 2 K. A structure where all spins lie inside the basal a_1a_2 plane yields the best result. Here we use the orthorhombic setting (space group $Fddd$) of the low-temperature structure with $a_1 \geq a_2 > a_3$. The net moment becomes 0.93(5) μ_{B} per formula unit (f.u.). A refinement with the ferrimagnetic moments directed along the tetragonal axis a_3 , as reported in Ref. [8], yields a net moment of 2.5 $\mu_{\text{B}}/\text{f.u.}$, which is much larger than 0.74 $\mu_{\text{B}}/\text{f.u.}$ observed in magnetization measurements [6]. Therefore, the latter model is discarded for CuCr_2O_4 . On the other hand, the reanalysis of the magnetic structures of $\text{Cu}_{0.8}\text{Ni}_{0.2}\text{Cr}_2\text{O}_4$ confirms the results reported earlier [8], where ferrimagnetism is now established with moments aligned along the tetragonal axis. Together with a new study on $\text{Cu}_{0.9}\text{Ni}_{0.1}\text{Cr}_2\text{O}_4$ it shows that 10 percent substitution of Cu by Ni is sufficient to reorient the ferrimagnetic moments. The spin arrangement on the Cr_4 tetrahedron

in CuCr_2O_4 is sketched in Fig. 1. The data analysis indicates that a magnetic structure with inverted ferrimagnetic spins, while retaining the Cr_{AF} mode, does not lead to a satisfying fit. We discuss this important result below.

Close to the paramagnetic state the ordered moments and their associated intensities are rather weak, and superimpose on nuclear intensities for particular reflections. Therefore, the results from simultaneous refinements of the nuclear and magnetic structure become more and more inaccurate, where the weight of prominent weak intensities is underestimated in the standard profile refinement, in particular if the full pattern is taken into account. Instead, for temperatures above 100 K, we follow the temperature behavior of integrated reflection intensities containing magnetic contributions. The data analysis simplifies due to extinction of particular reflections. Table I lists possible magnetic scattering for the three magnetic modes and additionally the presence of nuclear scattering. E.g., for Cr_{AF} , with moments lying in the a_1a_2 plane, only magnetic intensity is generated on the 002 reflection. Similarly, Cu_{F} is the only mode generating magnetic scattering superimposed on the nuclear 202/022 reflections. This allowed us to determine separately the individual moment values of these two modes.

The appearance of 002 below 155 K and the onset of magnetic scattering at 202/022 below 130 K indicate that Cr_{AF} emerges 25 K above the onset of the Cu_{F} mode (Figs. 2 and 3). Moreover, the measured intensity ratio $I(111)/I(002) = 1.65$ between 155 and 130 K implies the concomitant occurrence of the Cr_{AF} and Cr_{F} mode (Fig. 2), since the presence of the pure Cr_{AF} has $I(111)/I(002) = 1.18$. The measured value of 1.65 is constant between 155 and 130 K indicating Cr spin order with a moment canting of 20° , i.e. $m_{\text{AF}} = 2.8 m_{\text{F}}$. This is in contrast to the results given in Ref. [9], where the high temperature magnetic phase consists only of Cr_{AF} . However, a careful look to the low-angle part of the 138 K diffraction pattern (Fig. 2(a) of Ref. [9]) shows that this model generates too low intensity on 111, 220 and the pair 202/022, and too high intensity on 002. This indicates that a magnetic structure with Cr_{AF} only does not describe the measured pattern satisfactorily. The ratio $I(111)/I(002)$ becomes accessible from Fig. 2(b) of Ref. [9]. Calculation of $I(111)/I(002)$ for the ground-state model quoted in Ref. [9] yields a value of 2.4. Reading out an intensity ratio of $2/3$ for the normalized intensity around 138 K in Fig. 2(b) of Ref. [9] and multiplying $2/3$ by the factor 2.4 yields a value of 1.6 for $I(111)/I(002)$. This value strongly supports the presence of Cr_{F} in addition to Cr_{AF} .

Below 130 K the Cu mode adds on to the two Cr modes and we observe a gradual change of $I(111)/I(002)$ from 1.65 at 130 K to 2.25 at 105 K. The latter intensity ratio already corresponds to the value determined for the ground state, where all three modes are present. Beside the clear indication for the onset of magnetic Cu order below 130 K, the very weak

temperature variations in the 202/022 intensity down to 105 K, due to the poor statistics, are not taken into account for analyzing the temperature dependence of the Cu_F mode. Instead, magnetization measurements are performed to obtain further information on the ferrimagnetism (Fig. 4). The magnetization starts to increase below the high temperature (HT) transition at 155 K and arises from the Cr_F mode. At the low temperature (LT) transition around 130 K, with the onset of Cu_F , a point of inflection becomes visible in $m(T)$. The magnetization continuously increases towards lower temperature and approaches saturation below 20 K to a value of $0.67 \mu_B/\text{f.u.}$ The latter value is below $0.95(5) \mu_B/\text{f.u.}$ obtained from neutron diffraction. We note that m still increases slightly with applied field beyond 14 T. The measurements show a continuous increase in magnetization with lowering temperature i.e. $dm/dT < 0$ below 130 K. The magnitude of the magnetization, denoted by m , is the superposition of the coupled modes $m(\text{Cr}_F)$ and $m(\text{Cu}_F)$ i.e. $m = m(\text{Cr}_F) - m(\text{Cu}_F)$. The “minus” takes account of the FI spin arrangement. Therefore, $d[m(\text{Cr}_F)] > d[m(\text{Cu}_F)]$ below 130 K.

Next, we look at the two Ni-doped samples. In common with pure Cu chromite the onset of magnetic scattering on 002 (Cr_{AF}) occurs at higher temperature than on 202/022 (Cu_F). Differing is the ratio $I(111)/I(002)$ for the HT magnetic phase. The ratio changes from 1.65 for the Cu-sample to 1.3 for the Ni-doped samples. The latter value is still too large if only Cr_{AF} is present. The earlier refinement of $\text{Cu}_{0.8}\text{Ni}_{0.2}\text{Cr}_2\text{O}_4$ at 2 K indicates that the ferrimagnetic moments are aligned along the a_3 axis [8]. The same result is obtained in this work from the refinement of $\text{Cu}_{0.9}\text{Ni}_{0.1}\text{Cr}_2\text{O}_4$. Taking this into account we can directly determine the moment for Cr_F in the HT magnetic phase from the $I(111)/I(002)$ ratio for the Ni-doped samples. As a result, the canting angle of the moment is also close to 20° as was found for pure Cu-chromite. The obtained moments of Cr_{AF} and Cr_F are listed in Table II.

III. DISCUSSION

A. General

Ferrimagnetic normal spinels $AB_2\text{O}_4$ show one or more magnetic transitions. Frequently a HT ferrimagnetic phase is established by oppositely oriented F modes on the A and B sublattices, sometimes followed by a lower temperature AF transition resulting in canted moments on the B ions, magnetic spirals etc. [1]. Mean-field studies on the ground states of tetragonal spinels consider A - A , A - B and B - B interactions between nearest neighbors [15].

Stability regions for $\mathbf{k} = 0$ structures were identified as Néel, Yafet-Kittel, and colinear antiferromagnetic modes. The latter consider antiparallel configurations within both, the A and the B sublattice. In addition, it has been concluded that the ferrimagnetic Néel structure is always established at the HT transition, which can be followed by a LT transition to form a noncolinear structure like a canting of B moments for the Yafet-Kittel spin arrangement. Our experimental results on the spin order of CuCr_2O_4 show that mean-field calculations with nearest neighbor (nn) interactions at least fail to describe the observed sequence of transitions just mentioned.

We first discuss the Cr_{AF} mode, which dominates the magnetic structure. This mode has the largest moment and the highest ordering temperature. The Cr^{3+} ions are located on a tetragonally distorted tetrahedron (Fig. 1). Nearest neighbors are coupled antiferromagnetically via direct exchange and ferromagnetically by two superexchange paths via oxygen ions. For short Cr-Cr distances, the AF-direct exchange is stronger than the competing F-type superexchange [16]. In the flattened tetrahedron, the interactions split into four strong AF and two weak AF or even F bonds with Cr-Cr distances of 2.87 and 3.02 Å, respectively. Establishing the four strong AF bonds forces the weak bonds into a ferromagnetic alignment. This gives rise to a ferromagnetic spin arrangement inside the tetragonal layers. Electronic band structure calculations on chromites, containing nonmagnetic A^{2+} ions Zn, Cd, Hg, indicate a decrease in the value for J_1 with increasing Cr-Cr distance and a turnover from AF to F bonding for HgCr_2O_4 with $d_{\text{Cr-Cr}} = 3.06$ Å [16]. A significant AF bond between next nearest neighbors (nnn) along [100] and [010] for the space group $I4_1/amd$ is reported as well [16]. The nnn exchange J_3 competes with nn AF couplings J_1 and can give rise to helimagnetism in case J_3 becomes sufficiently large with respect to J_1 [17]. In a simple chain model, the absence of a helimagnetic structure requires $J_3 \leq 0.25 J_1$.

More challenging is the presence of the Cr_{F} mode in the absence of magnetic spin order for Cu between 130 and 155 K. This questions the common understanding that a strong AF coupling between the Cu_{F} and Cr_{F} modes is essential for establishing long-range order Cr_{F} order. The latter is the result of a mean-field calculation, in which the sublattices A and B are subdivided [10]. Qualitatively Cr_{AF} results from a strong nearest neighbor B - B coupling, which competes with the Cr_{F} mode coupled to the Cu_{F} mode via strong A - B coupling. The canting angle of the moments depends on the ratio of the two coupling strengths. There exist two possibilities to couple the two modes Cr_{F} and Cr_{AF} . Fixing the AF moments S_1 and S_4 along a_1 , and S_2 and S_3 along $-a_1$, the Cr_{F} moments can point along either the positive or the negative of the direction of the a_2 axis (Fig. 1). Neutron powder diffraction distinguishes between these two

cases as is illustrated for the structure factor of the 111 reflection. Along [111], the 3-dim. lattice consists of layers, alternating between a “Kagome-type” lattice, containing the three ions Cr₂, Cr₃, and Cr₄, and a triangular lattice occupied by Cr₁ ions. The phase shift between adjacent planes is π . (Fig. 1). Adding all spins for the four Cr ions, taking into account their phases, yields $2 S_{AF}$ and $2 S_F$ for the two modes, respectively. Here we have set the phase to zero on the Kagome-like plane. Next, one has to project $2 S_{AF}$ and $2 S_F$ onto the (111) scattering plane, because neutrons are only sensitive to this component (see lower part of Fig. 1). The obtained spin scattering amplitudes for the direct (solid red arrow) and for the inverted (broken red arrow) F mode are inclined to the AF amplitude by a smaller and a larger angle, respectively. Thus the measured intensity, which is proportional to the squared total amplitude (green arrows), becomes larger for the direct and smaller for the inverted F mode. The reflections related to the other members of $\langle 111 \rangle$, containing all body diagonals, behave identically. Simulations using the *FullProf* suite [13] confirm that the coupling of the modes Cr_{AF x} and Cr_{F y} , where x and y indicate the spin direction along the a_1 and a_2 axis, respectively. A similar analysis shows that only the coupling of Cr_{AF x} Cr_{F y} is consistent, and not $-Cr_{AFx}Cr_{Fy}$, with the observed intensities for 002 and 111.

B. Symmetric versus antisymmetric magnetic coupling

The magnetic structure consists of ferromagnetically ordered layers in the tetragonal plane. The magnetization rotates alternately clockwise and counterclockwise from layer to layer along a_3 . This spin arrangement can arise from a symmetric or antisymmetric coupling. The latter, given by

$$H_D = \mathbf{D} \cdot (\mathbf{S}_i \times \mathbf{S}_j),$$

occurs if no inversion center is midway the connecting line between two magnetic ions [18-19]. Applying Dzyaloshinskii-Moriya symmetry rules, considering the tilted CrO₆ octahedra, allow to specify possible axes for \mathbf{D} , however not the sign i.e. the direction of \mathbf{D} . The arrangements of \mathbf{D} vectors are similar to the ones considered for the investigation of magnetic structures on regular antiferromagnetic pyrochlore lattices [20]. Microscopically, nearest neighbor Cr _{i} and Cr _{j} ions, separated by \mathbf{r}_{ij} , couple via two bridging oxygen ions (Fig. 5). Then the presence of a mirror plane m_1 containing \mathbf{r}_{ij} and another plane m_2 perpendicular to \mathbf{r}_{ij} (Fig. 5(bottom)) determine the axis for the \mathbf{D} vector. Although antisymmetric coupling is active on the individual bonds, an appropriate summation, considering the four bonds coupling the planes along a_3 , does

not yield a \mathbf{D} vector along that direction. This result is supported by the observation that only the two couples $\text{Cr}_{\text{AFy}}\text{Cr}_{\text{Fx}}$ and $\text{Cr}_{\text{AFx}}\text{Cr}_{\text{Fy}}$ lead to the measured intensity ratio of 1.65 for $I(111)/I(002)$. Therefore, the Hamiltonian contains a symmetrical term $\text{Cr}_{\text{Fx}}\text{Cr}_{\text{AFy}} + \text{Cr}_{\text{Fy}}\text{Cr}_{\text{AFx}}$, and not $\text{Cr}_{\text{Fx}}\text{Cr}_{\text{AFy}} - \text{Cr}_{\text{Fy}}\text{Cr}_{\text{AFx}}$ which describes antisymmetric coupling [21].

The symmetrical coupling between two spins contains exchange and anisotropy [21]. For instance, single-ion anisotropy originates from ligand fields of oxygen ions situated around the magnetic Cr or Cu/Ni ions. The Cr ions lie in the center of a weakly disordered oxygen octahedron (Fig. 5). The three d electrons form an orbital (t_{2g})³ singlet so that the orbital angular momentum is quenched up to first-order-perturbation calculations [22] and one expects a spin only moment of about $3 \mu_{\text{B}}$ for the high-spin state. Anisotropy can still enter by partial restoration of orbital-angular momentum that appears in second-order-perturbation calculations. The neutron diffraction results indicate that the Cr_{AF} moments for all three specimens lie in the tetragonal plane. High-resolution powder diffraction experiments on CuCr_2O_4 revealed that the Cr_{AF} moments align along the largest lattice constant a_1 in the orthorhombic state [9]. An in-plane moment for Cr has also been found for the spinel ZnCr_2O_4 containing nonmagnetic Zn [23]. The lattice of this compound is very weakly flattened induced by a spin-Peierls-like transition. The Cr-Cr distance with 2.944 \AA is comparable to that of CuCr_2O_4 . This could indicate that magnetic anisotropy at the Cr site prefers an in-plane moment. Remarkable is the reorientation of the Cr_{F} component from in-plane for pure Cu chromite to the tetragonal direction a_3 for both Ni-doped samples, even above 130 K in the absence of long-range spin order on the Cu/Ni site. There is no indication for a change in lattice symmetry. An “out of the tetragonal plane” component for Cr is determined as well for the weak tetragonal CdCr_2O_4 with $a_3 > a_1$ [24]. A possible influence of the spin reorientation by the Cu/Ni concentration has probably to consider strains due to competing Jahn-Teller distortions with a contraction and elongation of one of the cubic axes for Cu and Ni, respectively [25].

C. Magnetoelasticity

A coupling between spins and lattice can be quite pronounced in magnetic oxides. We now compare the observed magnetic order with the thermal evolution of structural parameters as reported in [6]. For CuCr_2O_4 , the magnetic transition with the onset of canted Cr spin order coincides with kinks in the thermal evolution of the lattice parameters (Fig. 8 in Ref. [6]). The enforced increase of a_3 and decrease of a_1 indicate an additional tetragonal distortion, which is

superposed on the JT effect. An increased rate of the volume reduction is visible as well. The lattice deformations generated by the spin order are nearly linear dependent on temperature, similar to the behavior of the magnetic intensity. Hence, the magnetoelastic distortion is approximately proportional to the square of the magnetic order parameter. The magnetically induced tetragonal distortion for the upper transition can be attributed to direct nearest neighbor AF exchange between the Cr ions established by four strong magnetic AF bonds, which are selected by the tetragonal JT distortion [Fig. 1]. No orthorhombic distortion becomes visible, despite the onset of the ferromagnetic mode Cr_F .

However, a symmetry reduction from tetragonal to orthorhombic appears at the lower continuous transition with the onset of Cu_F -spin ordering. Our measurements do not allow to decide, whether only the Cu_F order or the ferrimagnetic spin arrangement formed by Cu_F and the already existing Cr_F mode accounts for the orthorhombic distortion.

Below 100 K the lattice distortion and the magnetic structure approach saturation (Fig. 8 of Ref. [6] and Fig. 2). Noticeable for the distortion is a freezing of one lattice constant within the basal plane (Fig. 8 of Ref. [6]). A similar behavior is observed for NiCr_2O_4 (Fig. 6 of Ref. [6]), where the basal plane is now formed by the long and short lattice constants for CuCr_2O_4 and NiCr_2O_4 , respectively. Between 155 and 130 K, solely Cr_F determines the evolution of the net moment. For 130 K the net moment is about $1 \mu_B$ which is close to the net moment for the ground state. Statistics of our diffraction data is insufficient to follow quantitatively the net moment during the temperature range between 130 and 105 K. The net moment seems to be weakly dependent on temperature below 130 K. This result differs from the outcome of the magnetization measurements. Here the net moment is significantly lower at all temperatures and the moment increases all the way down to the ground state. An inflection point in $M(T)$ indicates approximately the onset of Cu ordering. The difference in moment is most pronounced at higher temperatures especially at 130 K where magnetization yields only $0.3 \mu_B$ while neutrons yield $1 \mu_B$. At lower temperatures, the difference reduces roughly to one third. A lower value in the net moment by the magnetization measurements at powder samples can be related to the in-plane anisotropy of the Cr moments for CuCr_2O_4 .

Another signature for magnetoelasticity is seen by optical spectroscopy, which reveals a splitting of E_{2u} phonon modes for Cu chromite around 152 K (Fig. 9 of Ref. [26]). The phonon splitting is attributed to the ferrimagnetic transition. This temperature is close to T_{Cr} , where we observe the canted magnetic Cr order; however, there is no evidence for a symmetry reduction lower than tetragonal from synchrotron diffraction [6]. Differences in temperature calibration could be present if one considers the spinel NiCr_2O_4 , where the orthorhombic distortion occurs

at 65 K [6], although the phonon splitting by optical spectroscopy is found at 74 K [26]. Therefore, it is likely that the Cu ordering and the reported phonon splitting sets in at a temperature around 130 K and not 152 K. At this temperature the magnetic Cu ordering is accompanied by the onset of the orthorhombic lattice distortion [6] which probably accounts for the lifting of the two-fold degenerate E_u modes. It is stated in Ref. [26] that a first mode splitting at room temperature is already present due to the cubic to tetragonal Jahn-Teller transition at 854 K.

Finally, we compare the results on the determined magnetic structures with those obtained from the irreducible representation (Irrep) analysis for the tetragonal and orthorhombic space groups $I4_1/amd$ and $Fddd$, respectively, given in Ref. [9]. The magnetic ground state of CuCr_2O_4 can be associated to only one Irrep using the orthorhombic space group. This Irrep allows simultaneously the presence of ferrimagnetism by Cu_{Fy} and Cr_{Fy} , and antiferromagnetism by Cr_{AFx} . The situation changes for the Ni-doped samples. Due to the spin reorientation the ferromagnetic modes become Cu_{Fz} and Cr_{Fz} , while Cr_{AFx} remains unchanged. No Irrep can now be associated with the determined magnetic structure. A similar result with respect to CuCr_2O_4 and the Ni-doped specimens is obtained for the HT magnetic phase using space group $I4_1/amd$ (Table III). Since increasing Ni-doping introduces a local orthorhombic distortion the presence of an averaged weak orthorhombic distortion in our Ni-doped samples becomes possible. This does not change the result that the magnetic structure in the Ni-doped specimens cannot be attributed to any Irrep of $Fddd$ or $I4_1/amd$.

III. SUMMARY AND CONCLUSION

We give a detailed description of the temperature dependence of the three magnetic modes in CuCr_2O_4 . The spin canting on the Cr sublattice sets in at 155 K, while the Cu_{F} mode establishes below 130 K. In mean-field calculations [10] the canting of Cr moments is attributed to a competition between the AF mode by nearest-neighbor exchanges on a single Cr tetrahedron, and the antiparallel coupling between the Cu_{F} and the Cr_{F} modes. Therefore, the calculated triangular spin arrangement, established by the canted Cr-modes, necessitates the Cu_{F} mode in order to realize Cr_{F} . Our analysis shows a symmetrical coupling of Cr_{AF} and Cr_{F} modes. Hence, a Dzyaloshinskii-Moriya interaction with an antisymmetric coupling cannot account for the observed alternating clockwise and counterclockwise spin rotations along a_3 .

The tilting of the oxygen octahedra is considerably less than the moment canting, and single-ion anisotropy is not responsible for the canting. Competing interactions between nn and nnn, which frequently create spiral spin arrangements [17], do not allow spin canting. Hence, the origin for the spin canting remains unsolved.

The moment direction for the Cr_F mode depends on the concentration x on the A site in $\text{Cu}_{1-x}\text{Ni}_x\text{Cr}_2\text{O}_4$. The Cr_F moment lies inside the tetragonal plane for $x = 0$, however points along the tetragonal axis for $x = 0.1, 0.2$. The spin orientation does not change across the high temperature – low temperature transition. A 10% substitution of Cu by Ni affects marginally the tetragonal crystal symmetry. Our results together with outcomes reported in [8,9] indicate that the Cr_{AF} moments for $\text{Cu}_{1-x}\text{Ni}_x\text{Cr}_2\text{O}_4$ always align along the largest lattice constant.

The determined magnetic order transitions correlate with changes in the crystal structure [6]. The origin of the orthorhombic distortion at the low temperature transition is associated either with the spin ordering of the Cu/Ni ions alone, or with the formation of the ferrimagnetic structure involving Cr_F as well. Although our measurements do not allow inferring magnetic exchange constants, they can provide a fruitful testing ground for DFT calculations, which predict exchange constants [27].

Beside the unusual magnetic behavior of CuCr_2O_4 it has been reported recently that a ferroelectric order with a polarization of $0.15 \mu\text{C cm}^{-2}$ occurs at a temperature around 170 K [28]. A transition to a polar structure with a space group *Ima2* becomes evident for Co-doped copper chromites. This indicates the presence of a complex and fascinating interplay between lattice, magnetic and ferroelectric properties.

ACKNOWLEDGEMENT

The authors thank R. Feyerherm for critical reading of the manuscript and valuable discussions.

References

[1] H. Takagi and S. Niitaka, Highly frustrated magnetism in spinels, in *Introduction to Frustrated Magnetism*, edited by C. Lacroix, P. Mendels, F. Mila, Springer Series in Solid State Science 164 (Springer, Berlin, Heidelberg, 2011).

- [2] J. T. Chalker, Geometrically Frustrated Antiferromagnets: Statistical Mechanics and Dynamics, in *Introduction to Frustrated Magnetism*, edited by C. Lacroix, P. Mendels, and F. Mila, Springer Series in Solid State Science **164**, 3 (2011).
- [3] L. Balents, Nature **464**, 207 (2010).
- [4] S. C. Tarantino, M. Giannini, M. A. Carpenter, and M. Zema, IUCrJ **3**, 354-366 (2016).
- [5] M. Tovar, R. Torabi, C. Welker, and F. Fleischer, Phys. B: Condens. Matter **385-386**, 196-198 (2006).
- [6] M. R. Suchomel, D. P. Shoemaker, L. Ribaud, M. C. Kemei, and R. Seshadri, Phys. Rev. B **86**, 054406 (2012).
- [7] E. Prince, Acta. Cryst. **10**, 554 (1957).
- [8] M. Reehuis, M. Tovar, D. M. Többens, P. Pattison, A. Hoser, B. Lake, Phys. Rev. B **91**, 024407 (2015).
- [9] K. Tomiyasu, S. Lee, H. Ishibashi, Y. Takahashi, T. Kawamata, Y. Koike, T. Nojima, S. Torii, and T. Kamiyama <https://arxiv.org/abs/1803.06447v1>
- [10] Y. Yafet and C. Kittel, Phys. Rev. **87**, 290 (1952).
- [11] T.A. Kaplan and N. Menyuk, Phil. Mag. **87**, 3711 (2007).
- [12] https://www.helmholtz-berlin.de/media/media/nutzerdienst/experimental_facilities
- [13] J. Rodríguez-Carvajal, Physica B **192**, 55 (1993).
- [14] N. Stüsser, M. Reehuis, M. Tovar, B. Klemke, A. Hoser, and J.-U. Hoffmann, Phys. Rev. B **98**, 144424 (2018).
- [15] N. Menyuk, K. Dwight, D. Lyons, and T. A. Kaplan, Phys. Rev., **127**, 1983 (1962).
- [16] A. N. Yaresko, Phys. Rev. B **77**, 115106 (2008).
- [17] J. S. Smart, *Effective Field Theories of Magnetism*, (W. B. Saunders Company, Philadelphia & London, 1966).
- [18] T. Moriya, Phys. Rev. **120**, 91 (1960).
- [19] I. E. Dzyaloshinskii, J. Phys. Chem. Solids **4**, 241 (1958).
- [20] M. Elhajal, B. Canals, R. Sunyer, C. Lacroix, Phys. Rev. B **71**, 094420 (2005).
- [21] E. F. Bertaut, Spin Configurations of Ionic Structures: Theory and Practice, in *Magnetism III*, edited by G. T. Rado, and H. Suhl, (Academic Press, New York, London, 1963).
- [22] H. L. Schäfer and G. Gliemann, *Basic Principle of Ligand Field Theory*, (Wiley-Interscience, New York, 1969).
- [23] S.-H. Lee, W. Ratcliff II, Q. Huang, T. H. Kim, S.-W. Cheong, Phys. Rev. B **77**, 014405 (2008).

- [24] J.-H. Chung, Y. S. Song, S. Ueda, Y. Ueda, and S.-H. Lee, *J. Kor. Phys. Soc.* **62**, 1900 (2013).
- [25] M. Kataoka and J. Kanamori, *J. Phys. Soc. Jpn.* **32**, 113 (1972).
- [26] V. Kocsis, S. Bordács, D. Varjas, K. Penc, A. Abouelsyed, C. A. Kuntscher, K. Ohgushi, Y. Tokura, and I. Kezsmarki, *Phys. Rev. B* **87**, 064416 (2013).
- [27] I. Efthimiopoulos, I. Khatri, Z. T. Y. Liu, S. V. Khare, P. Sarin, V. Tsurkan, A. Loidl, D. Zhang, and Y. Wang, *Phys. Rev. B* **97**, 184435 (2018) and Supplementary Information.
- [28] A. Chatterjee, J. K. Dey, S. Majumdar, A.-C. Dippel, O. Gutowski, M. v. Zimmermann, and S. Giri, *Phys. Rev. Mat.* **3**, 104403 (2019).

TABLE I. Magnetic intensities of low-order reflections in the HT magnetic phase at 137 K generated by possible modes or phases of CuCr_2O_4 . The hyphens label the extinct intensity of reflections for different modes. The intensities I_{nuc} for the nuclear reflection are also listed.

	$I(111)$	$I(002)$	$I(202/022)$	$I(111)/I(002)$
Cu_F	0	–	0 [Fig. 3]	–
Cr_F	120	–	–	–
Cr_{AF}	3800	3300	–	1.16
Cr_{AF} & Cr_F	5500	3300	–	1.65
I_{nuc}	120	0	11600	–

TABLE II. Intensity ratios $I(111)/I(002)$, determined moments of Cr_{AFx} , Cr_{Fy} or Cr_{Fz} , and the corresponding canting angles for pure and Ni-doped Cu chromite given for the HT magnetic phase.

Sample	T	$I(111)/I(002)$	Cr_{AFx}	Cr_{Fy}	Cr_{Fz}	Canting angle
CuCr_2O_4	137 K	1.65	$1.29 \mu_B$	$0.46 \mu_B$	–	20°
$\text{Cu}_{0.9}\text{Ni}_{0.1}\text{Cr}_2\text{O}_4$	136 K	1.3	$1.23 \mu_B$	–	$0.46 \mu_B$	20°
$\text{Cu}_{0.9}\text{Ni}_{0.1}\text{Cr}_2\text{O}_4$	125 K	1.3	$1.6 \mu_B$	–	$0.61 \mu_B$	21°
$\text{Cu}_{0.8}\text{Ni}_{0.2}\text{Cr}_2\text{O}_4$	125 K	1.3	$1.3 \mu_B$	–	$0.53 \mu_B$	22°

TABLE III. Irrep for $I4_1/amd$ allowing Cr_{AFx} , Cr_{Fy} , in the HT magnetic phase choosing $p = -r$, $w = u$, and $v = q = 0$.

CuCr_2O_4	Spin components	Cr_{AFx}	Cr_{Fy}	Cr_{Fz}
$\text{Cr}_1 (0\ 0\ 0)$	(r, u, v)	r	p	0
$\text{Cr}_1 (\frac{1}{2}\ 0\ \frac{1}{2})$	$(r, u, -v)$	r	p	0
$\text{Cr}_1 (\frac{1}{4}\ \frac{3}{4}\ \frac{1}{4})$	$(p, w, -q)$	$-r$	p	0
$\text{Cr}_1 (\frac{1}{4}\ \frac{1}{4}\ \frac{3}{4})$	(p, w, q)	$-r$	p	0

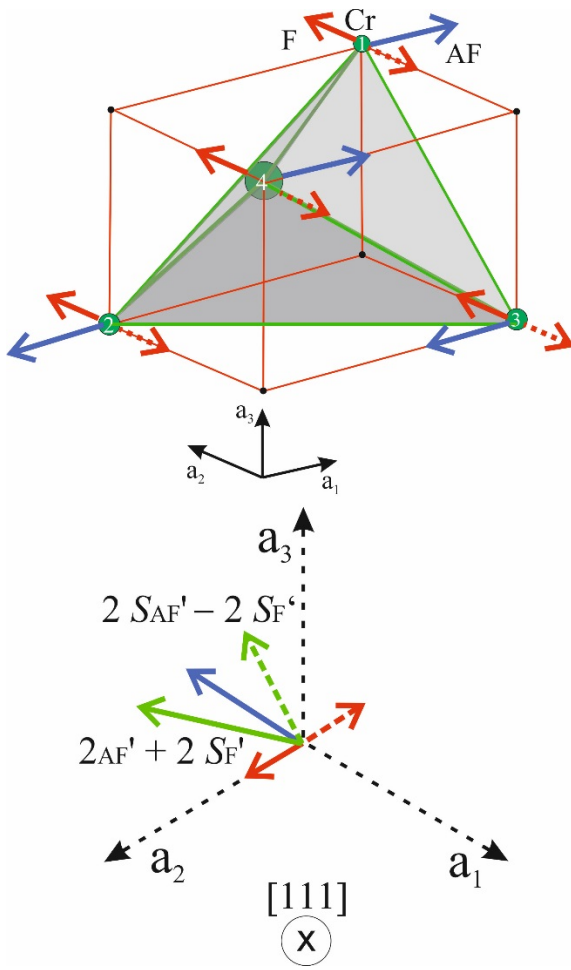


FIG. 1. Magnetic structure on the Cr_4 tetrahedron. Blue arrows indicate the Cr_{AFx} mode. The red solid and broken arrows show the two possible Cr_{Fy} modes, respectively. In the lower part, we show the projection of $2S_{AFx}$ and $2S_{Fy}$ on the (111) scattering plane as explained in the text.

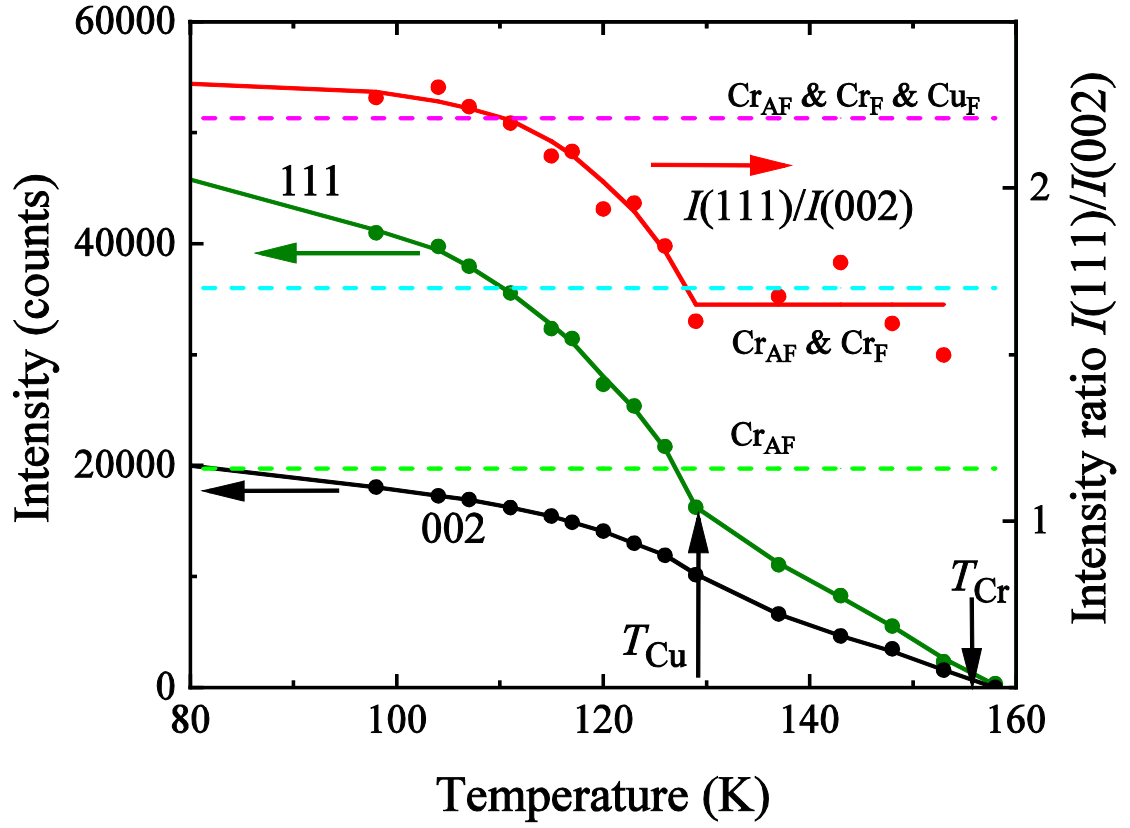


FIG. 2. Intensity versus temperature for 111 and 002 reflections, together with intensity ratio $I(111)/I(002)$ for CuCr_2O_4 . Horizontal lines show $I(111)/I(002)$ for the magnetic ground state with presence of Cr_{AF} , $\text{Cr}_{\text{AF}} \& \text{Cr}_{\text{F}}$, or $\text{Cr}_{\text{AF}} \& \text{Cr}_{\text{F}} \& \text{Cu}_{\text{F}}$.

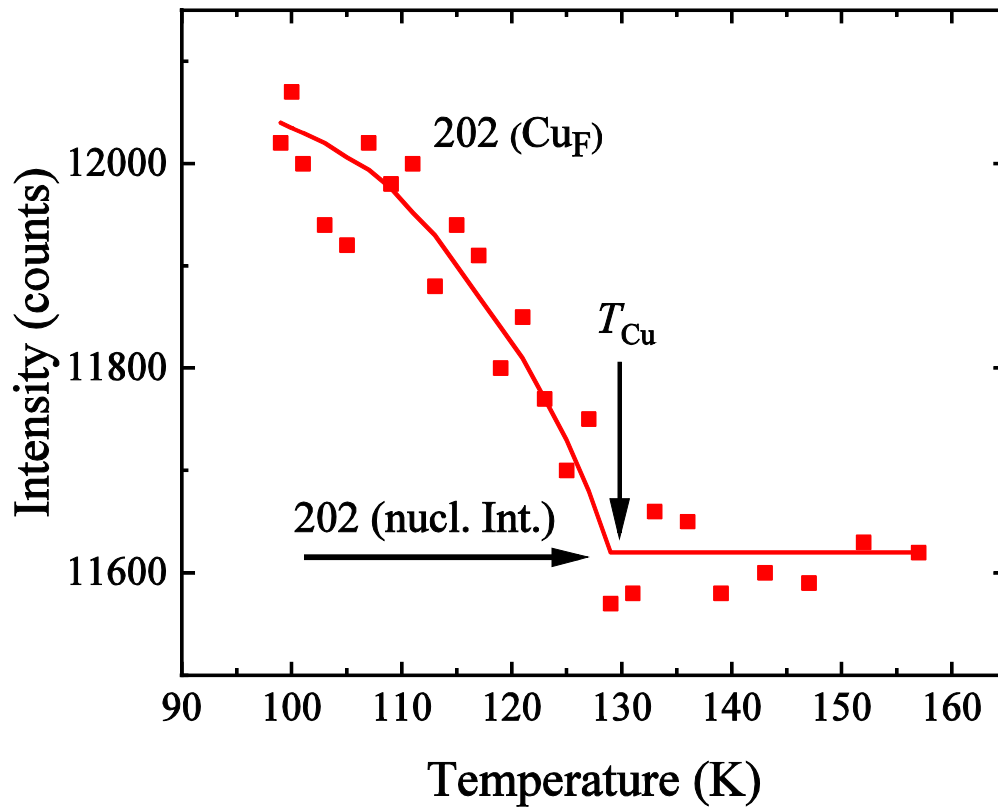


FIG. 3. Intensity of the pair 202/022 of CuCr_2O_4 versus temperature showing magnetic scattering by the onset of ferromagnetic order on the Cu sublattice. The statistical error for the counts is about 1%. The black horizontal arrow indicates the nuclear intensity of 202/022.

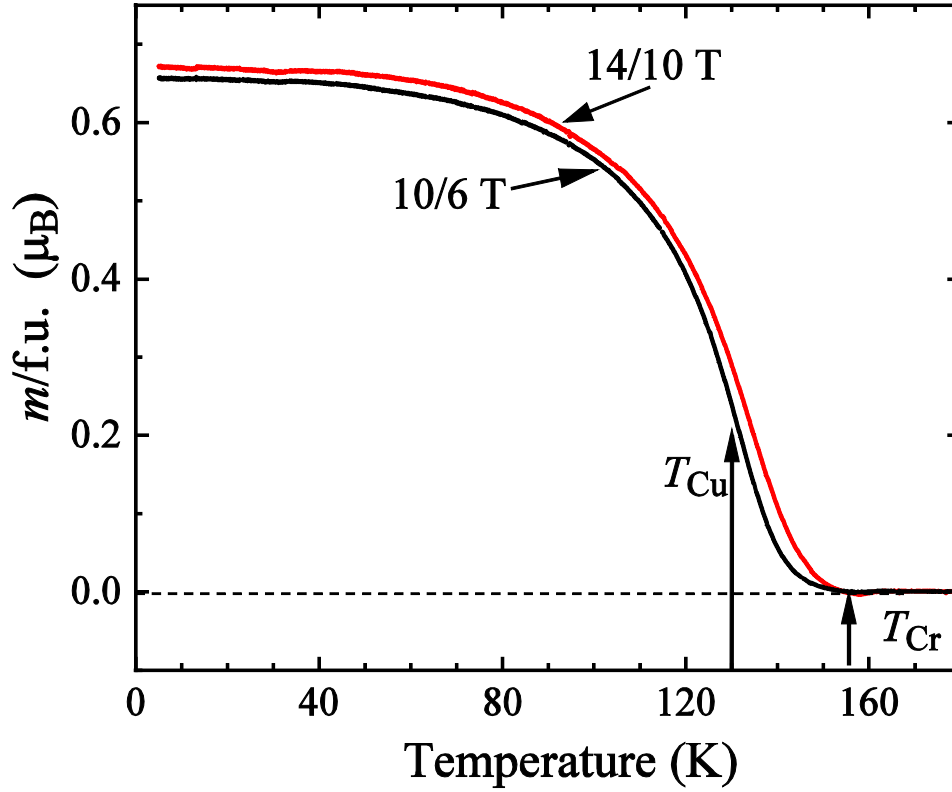


FIG. 4. Temperature dependent net magnetization m of CuCr_2O_4 determined from m_{H_2} and m_{H_1} using $m = m_{H_1} - (m_{H_2} - m_{H_1}) * H_1 / (H_2 - H_1)$ with applied fields indicated by H_2/H_1 . Here m_{H_i} denotes the temperature dependent magnetization carried out applying a field of strength H_i . E.g. the red curve is obtained using measurements performed at 10 and 14 T. The magnetization $m(T)$ at zero field is obtained from a linear extrapolation according to the above equation.

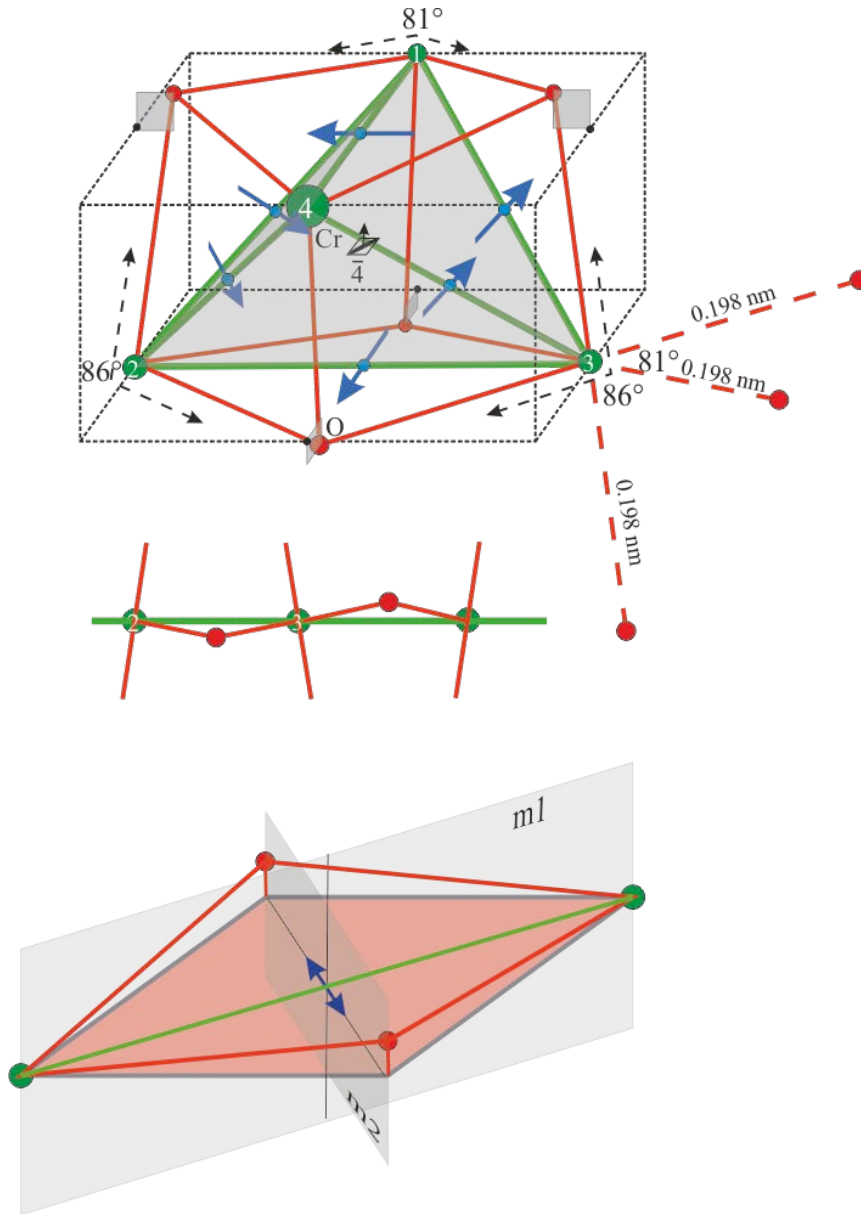


FIG. 5. Top: Cr_4 tetrahedron (green) and Cr_4O_4 polyhedron showing superexchange paths Cr-O-Cr (red lines). Distorted octahedral oxygen is sketched for Cr_3 ion. The cuboid (broken line) circumscribes the tetrahedron. Small grey areas indicate an out of plane shift of oxygen ions from the cuboid. Then, the quadrilateral Cr-O-Cr-O is formed by two equal sized Cr-O-Cr triangles inclined to each other (bottom and center). This breaks inversion symmetry and illustrates the possible antisymmetric interaction (blue arrows). The tetragonal symmetry differentiates between the Cr pairs 1-4, 2-3 inside tetragonal planes and the four other pairs coupling Cr spins located on adjacent tetragonal planes like 1-2. A few symmetry elements labelled m , 2 , and $\bar{4}$ are shown as well, because they become important in the identification of antisymmetric exchange (see text).